SANDIA REPORT

SAND2013-8156
Unlimited Release
September 2013

Laser-Ablated Active Doping Technique for Visible Spectroscopy Measurements on Z

Matthew Robert Gomez

Prepared by
Sandia National Laboratories
Albuquerque, New Mexico 87185 and Livermore, California 94550

Sandia National Laboratories is a multi-program laboratory managed and operated by Sandia Corporation, a wholly owned subsidiary of Lockheed Martin Corporation, for the U.S. Department of Energy's National Nuclear Security Administration under contract DE-AC04-94AL85000.

Approved for public release; further dissemination unlimited.

Sandia National Laboratories

Issued by Sandia National Laboratories, operated for the United States Department of Energy by Sandia Corporation.

NOTICE: This report was prepared as an account of work sponsored by an agency of the United States Government. Neither the United States Government, nor any agency thereof, nor any of their employees, nor any of their contractors, subcontractors, or their employees, make any warranty, express or implied, or assume any legal liability or responsibility for the accuracy, completeness, or usefulness of any information, apparatus, product, or process disclosed, or represent that its use would not infringe privately owned rights. Reference herein to any specific commercial product, process, or service by trade name, trademark, manufacturer, or otherwise, does not necessarily constitute or imply its endorsement, recommendation, or favoring by the United States Government, any agency thereof, or any of their contractors or subcontractors. The views and opinions expressed herein do not necessarily state or reflect those of the United States Government, any agency thereof, or any of their contractors.

Printed in the United States of America. This report has been reproduced directly from the best available copy.

Available to DOE and DOE contractors from
U.S. Department of Energy
Office of Scientific and Technical Information
P.O. Box 62
Oak Ridge, TN 37831

Telephone: (865) 576-8401
Facsimile: (865) 576-5728
E-Mail: reports@adonis.osti.gov
Online ordering: http://www.osti.gov/bridge

Available to the public from
U.S. Department of Commerce
National Technical Information Service
5285 Port Royal Rd.
Springfield, VA 22161

Telephone: (800) 553-6847
Facsimile: (703) 605-6900
E-Mail: orders@ntis.fedworld.gov
Online order: http://www.ntis.gov/help/ordermethods.asp?loc=7-4-0#online

SAND2013-8156
Unlimited Release
September 2013

Laser-Ablated Active Doping Technique for Visible Spectroscopy Measurements on Z

Matthew Robert Gomez
Radiation & Fusion Experiments
Sandia National Laboratories
P.O. Box 5800
Albuquerque, New Mexico 87185-MS1193

Abstract

Visible spectroscopy is a powerful diagnostic, allowing plasma parameters ranging from temperature and density to electric and magnetic fields to be measured. Spectroscopic dopants are commonly introduced to make these measurements. On Z, dopants are introduced passively (i.e. a salt deposited on a current-carrying surface); however, in some cases, passive doping can limit the times and locations at which measurements can be made. Active doping utilizes an auxiliary energy source to disperse the dopant independently from the rest of the experiment. The objective of this LDRD project was to explore laser ablation as a method of actively introducing spectroscopic dopants. Ideally, the laser energy would be delivered to the dopant via fiber optic, which would eliminate the need for time-intensive laser alignments in the Z chamber. Experiments conducted in a light lab to assess the feasibility of fiber-coupled and open-beam laser-ablated doping are discussed.

ACKNOWLEDGMENTS

I would like to acknowledge the PEs who allowed ride-a-long measurements during their Z shots which benefited this project. Additionally, I would like to thank Mike Cuneo who suggested that I pursue this research, and Yitzhak Maron and colleges from the Weizmann Institute of Science who have conducted similar research and provided guidance as to the general direction of the project.

Sandia National Laboratories is a multi-program laboratory managed and operated by Sandia Corporation, a wholly owned subsidiary of Lockheed Martin Corporation, for the U.S. Department of Energy's National Nuclear Security Administration under Contract DE-AC04-94AL85000.

This work was funded under LDRD Project Number 158701 and Title "Laser-Ablated Active Doping Technique for Visible Spectroscopy Measurements on Z".

CONTENTS

1. Introduction 9

2. Experimental Configuration 9

3. Experimental Results 11
   3.1. Laser Energy Vs. Internal Attenuator 11
   3.2. Laser Fiber Optic Coupling 13
   3.3. Open-Beam Experiments 15

4. Conclusions and Future Work 21

5. References 22

Distribution 23

FIGURES

Figure 1. (a) a schematic diagram showing the setup for the laser power measurements. (b) a schematic diagram showing the setup for the laser fiber optic coupling experiments. (c) a schematic diagram showing the setup for the open-beam plasma-generating experiments. 10
Figure 2. (a) a schematic diagram showing the vacuum chamber and diagnostic arrangement for the open-beam experiments that used the spectrometer and pinhole camera. (b) a schematic diagram showing the vacuum chamber and diagnostic arrangement for the open-beam experiments that used laser shadowgraphy. 11
Figure 3. A plot of the laser energy as a function of the internal attenuator setting. For attenuator settings above ~400, the trend is roughly linear. 13
Figure 4. A plot of the energy exiting the fiber as a function of the energy exiting the laser. The trend is approximately linear until the laser energy exceeds about 1.2 mJ 14
Figure 5. A plot of the maximum spot size as a function of laser energy that will punch a hole in a 0.8 µm thick aluminum foil 15
Figure 6. An open pinhole image of the laser striking the aluminum target and the resultant plasma plume. The scattered laser light is much brighter than the plasma plume so the plume is not observed. 16
Figure 7. (a) An open pinhole image of the plasma plume from the aluminum target. The target has been modified to block out the scattered laser light and the camera sensitivity has been increased. (b) An open pinhole image of the copper target with the same modifications to the target and camera. Note that the aluminum plume is blue-violet and the copper plume is blue-green. 17
Figure 8. A shadowgraph of the aluminum target during a shot. The plume is not obvious in this image, which is likely due to the diagnostic not registering the low density plasma. 18
Figure 9. A plot of the spectrum from the aluminum 5056 target. Two strong aluminum neutral lines are observed around 394 nm and 396 nm, and 3 weak magnesium neutral lines are observed around 383 nm. 19
Figure 10. A plot of the spectrum from the copper target. Three strong copper neutral lines are observed around 510 nm, 515 nm, and 522 nm. The background slopes upward at the long wavelength end of the spectrum due to scattered laser light (532 nm). 20

Figure 11. A plot of the spectrum from the sodium chloride and glue target. Two weak sodium neutral lines are observed around 589 nm. The signal to noise ratio for this target was only ~ 5. 21

TABLES

Table 1. Average laser energy as a function of internal attenuator setting..... 12

NOMENCLATURE

D_2	Deuterium gas
dB	decibel
H_2	Hydrogen gas
km	kilo-meter
Kr	Krypton
µJ	micro-Joule
m	meter
mJ	milli-Joule
mm	milli-meter
ng	nano-gram
nm	nano-meter
ns	nano-second
Std Dev	standard deviation
W	Watt
Z	The Z Machine

1. INTRODUCTION

Visible spectroscopy is used to measure plasma parameters including but not limited to: electron density, electron temperature, bulk plasma velocity, electric field, magnetic field, and plasma ionization states. On Z, these measurements are conducted on a wide variety of sources ranging from plasma in the power flow region of the accelerator, to plasma in H_2 gas cells, to emission from shocks in dynamic material physics experiments. In some cases, the desired parameter cannot easily be determined from the sample emission/absorption. This issue is solved by introducing a small quantity of another material (dopant) that allows the desired measurement to be made.

Dopants can be introduced actively or passively. To date, only passive dopants have been used on Z. A few examples of passive dopants are including 0.2% Kr in a D_2 gas fill for an inertial confinement fusion target or applying ~1-5 ng of sodium to a power flow surface. These dopants are considered passive because they are applied at a specific location and rely on the Z current pulse to move them to the desired location and produce the conditions required for emission/absorption. For example, the sodium on the power flow surface will not ablate and form plasma until the energy deposited by the current pulse exceeds a threshold.

Active dopants rely on a separate power source to either deliver the dopant to the region of interest (i.e. dopant gas injection system) or to produce the conditions required for emission/absorption (i.e. laser ablation) [1]. In some cases the active doping source is used to both deliver the dopant and produce the proper conditions. This is of particular interest if the region of interest is far from surfaces and in regions of low current density, which limits the use of passive dopants to late times. An example of such a region is the post-hole convolute.

This report discusses a series of experiments conducted in a light lab to determine the feasibility of active doping through laser-ablation. Experiments were conducted to test fiber-optic coupling of the laser pulse. Additional measurements of open-beam laser-ablation of several materials were also conducted.

2. EXPERIMENTAL CONFIGURATION

These experiments utilized a frequency-doubled Nd:YAG laser (NewWave Research – Tempest). The laser had a maximum energy per pulse of 100 mJ at a wavelength of 532 nm. The system included a variable internal attenuator allowing the energy to be adjusted from 10 µJ to 100 mJ. The full width at half maximum of the laser pulse was 4 ns. The laser was used in single pulse mode, but could be rep-rated up to 10 shots/second.

The laser system was set up in three distinct configurations as shown in figure 1. The first configuration (1a) was used to measure the laser energy as a function of the internal attenuation setting. The second configuration (1b) was used to assess the feasibility of fiber optically coupling the laser pulse. The third configuration (1c) was used to test the open-beam ablation configuration.

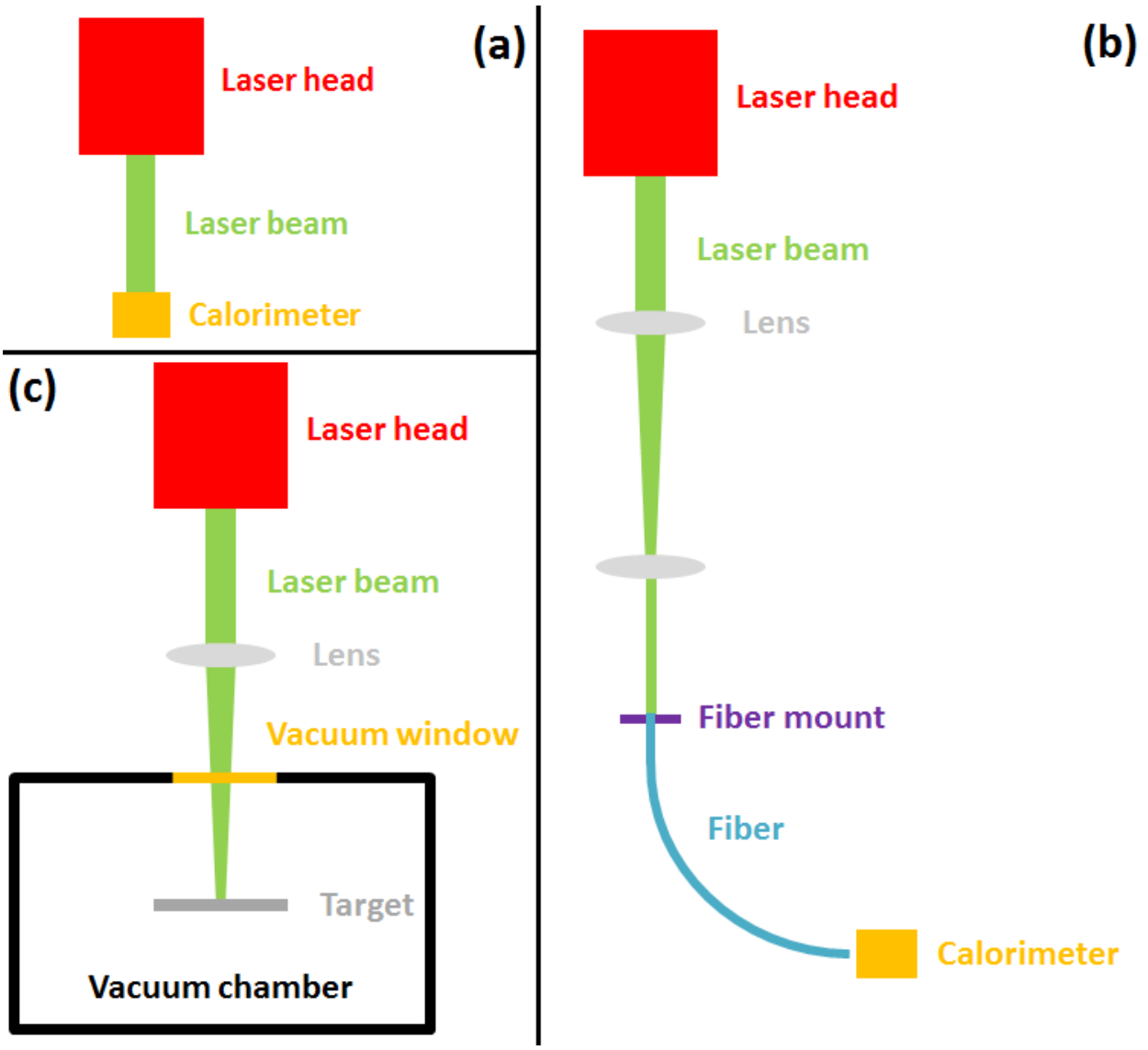

Figure 1. (a) a schematic diagram showing the setup for the laser power measurements. (b) a schematic diagram showing the setup for the laser fiber optic coupling experiments. (c) a schematic diagram showing the setup for the open-beam plasma-generating experiments.

A vacuum system was constructed for these experiments which allowed for a variety of diagnostic configurations. The vacuum and diagnostic systems are shown in figure 2. The diagnostics included time-integrated visible pinhole imaging, time-resolved laser shadowgraphy imaging, and time-integrated visible spectroscopy.

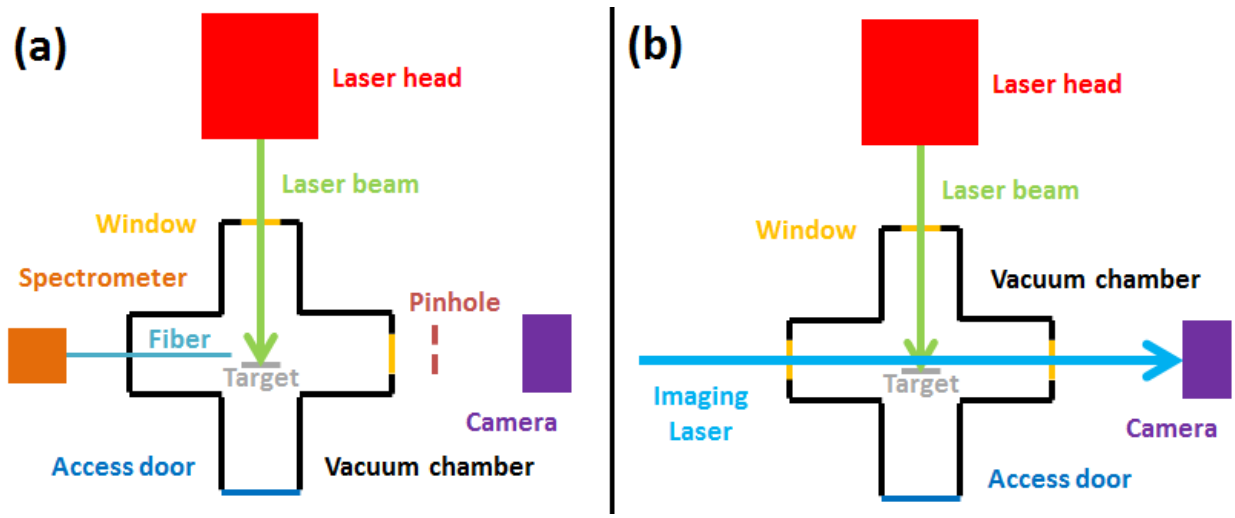

Figure 2. (a) a schematic diagram showing the vacuum chamber and diagnostic arrangement for the open-beam experiments that used the spectrometer and pinhole camera. (b) a schematic diagram showing the vacuum chamber and diagnostic arrangement for the open-beam experiments that used laser shadowgraphy.

Two types of targets were used in these experiments. One target was a solid piece of the dopant material. This target could be shot repetitively with the laser without the need to replace it after each shot. Aluminum, copper, and sodium targets of this type were used. The second type of target was a 0.8 µm thick aluminum foil. This target is of interest because it may reduce the energy threshold required to produce the dopant plume. The thin foil target required venting the vacuum system and replacing the target after each shot.

3. EXPERIMENTAL RESULTS

3.1. Laser Energy Vs. Internal Attenuator

Experiments were conducted to determine the linearity of the laser energy with the internal attenuator setting as well as to determine the shot-to-shot consistency of the laser energy. These experiments were conducted by firing the laser directly into a calorimeter (Gentec-e QE25LP-S-MB-D0). At each attenuator setting, the laser was fired in single shot mode a total of 20 shots, and the energy per pulse was recorded. The attenuator settings used, the average laser energy, and the standard deviation of the energy are listed in table 1.

The variations in the laser energy at a fixed attenuator setting were always less than 10%, and on average were approximately 5%. The largest variations were observed at the lowest laser energies, which were at the limit of the resolution of the calorimeter. At laser energies above 5 mJ the variations were 5% or less, and above 20 mJ they were closer to 3%.

The laser energy was not linearly related to the attenuator setting at low energies, but was very close to linear at energies above ~ 15 mJ. A plot of the average laser energy as a function of attenuator setting is shown in figure 3.

Table 1. Average laser energy as a function of internal attenuator setting.

Internal Attenuator	Average Laser Energy [μJ]	Std Dev of Laser Energy [μJ]
10	9.9	0.9
20	11.1	0.9
30	12.3	0.9
40	20.7	1.1
50	24.3	1.6
60	34.3	2.2
70	58.4	4.5
80	84.1	4.9
90	141	9
100	177	12
110	224	14
120	325	24
130	425	24
140	555	31
150	735	35
160	976	64
170	1181	72
180	1458	68
190	1750	97
200	2000	150
220	2790	160
240	4030	280
260	5290	270
280	6620	200
300	8040	310
325	10870	450
350	13180	650
375	15850	550
400	19260	560
500	34000	1100
550	42200	1000
600	50500	1400

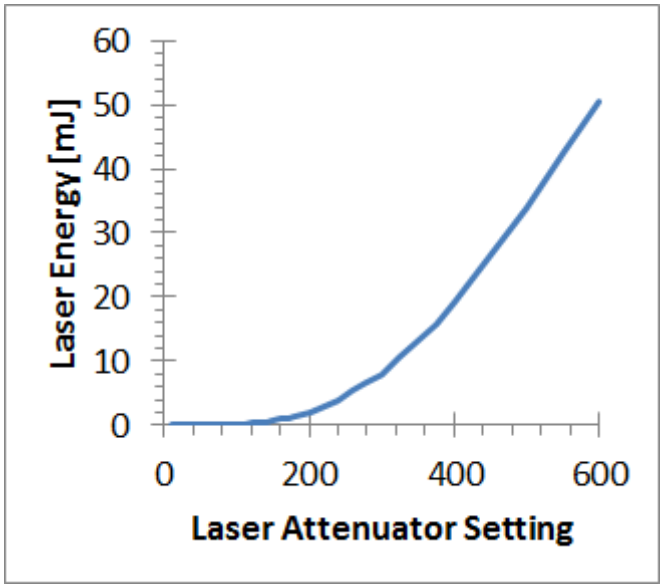

Figure 3. A plot of the laser energy as a function of the internal attenuator setting. For attenuator settings above ~400, the trend is roughly linear.

3.2. Laser Fiber Optic Coupling

These experiments utilized a 600 µm diameter core fiber (High OH Polymicro FVP600660710). Fiber optic coupling of laser light can be limited by damage to the surface of the fiber, damage to the bulk fiber material, fiber damage due to self-focusing, or fiber damage due to heating of surrounding materials (i.e. buffer, epoxy, etc.).

According to [2] for a polished fiber surface, the surface damage threshold can be as high as ~ 1000 mJ/mm^2. This indicates that a 600 µm diameter core fiber can accept > 280 mJ. The fiber was composed of fused silica, which has a bulk damage threshold of ~ 300 mJ/mm^2 [3]. This indicates that a 600 µm diameter core fiber can accept > 80 mJ. Self-focusing of laser light in a material can be calculated with

$$B = 2\pi/\lambda \int n_2 * I(z) dz \qquad (1)$$

where λ is the wavelength of the light, n_2 is the nonlinear index quantifying the Kerr nonlinearity, I(z) is the intensity of the laser, and dz is the distance along the fiber. The following values are fixed: B ~ 3, λ = 532 nm, n_2 = 2.5e-20 m^2/W, and $\int dz$ = 5 m. Thus the laser energy per pulse must be less than 2.3 mJ to avoid self-focusing. Heating of surrounding materials can be avoided by not allowing the laser to strike those materials. This can be accomplished by focusing the laser to slightly smaller than the fiber diameter or by removing/not including the materials. Based on all of these constraints, the maximum allowable incident laser energy was 2.3 mJ. By increasing the pulse duration to ~200 ns, the B integral can be increased to ~ 100 mJ.

The laser was focused using a plano-convex lens (300, 400, and 500 mm focal lengths tested) and re-collimated using a -50 mm focal length plano-concave lens. The collimated light was

directed onto the surface of the fiber, which was precisely positioned using an x-y translation stage. The laser energy exiting the other end of the fiber was measured using the calorimeter. A plot of the average output laser energy as a function of input laser energy is shown in figure 4. Roughly 60% of the laser energy was measured at the end of the fiber. The losses are a combination of reflections off of the two lenses (4 surfaces at ~4% reflections per surface), reflections off of the fiber surfaces (2 surfaces at ~4% reflections per surface), fiber attenuation (15 dB/km for 7 m), and imperfect coupling into the front of the fiber. Reflections account for approximately 22% of the loss and fiber attenuation accounts for 2% of the loss, so the imperfect coupling accounts for ~ 15%.

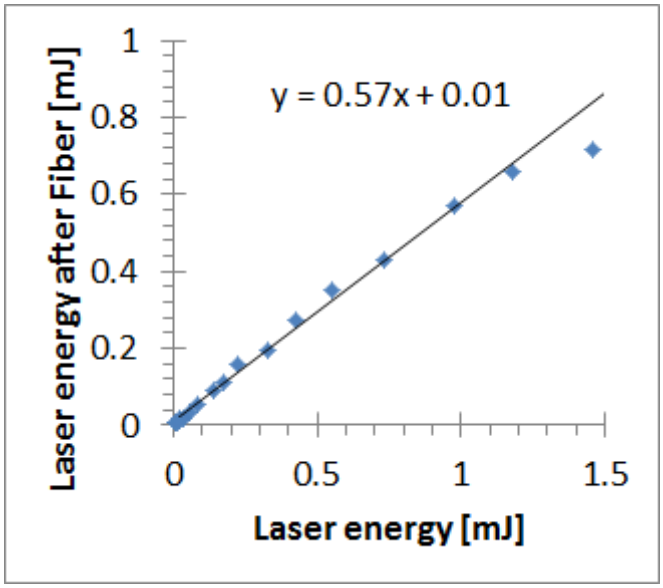

Figure 4. A plot of the energy exiting the fiber as a function of the energy exiting the laser. The trend is approximately linear until the laser energy exceeds about 1.2 mJ.

As the input power was increased above 1.2 mJ, the laser energy at the output end of the fiber dropped significantly. This is a factor of 2 below the expected damage threshold. Examination of the end of the fiber revealed localized regions on the surface that has been damaged. This indicated that there may be localized regions of the beam with intensities much higher than the average beam intensity. To verify this, the beam was passed through the plano-concave lens and the expanded image showed localized bright regions that matched the damage locations of the surface of the fiber.

A spatial filter was utilized in an attempt to improve the beam quality. The beam was focused with the 400 mm focal length plano-convex lens, and a 50 µm diameter high power spatial filter was placed at the beam focus. Unfortunately the laser intensity exceeded the breakdown threshold in air (2e11 W/mm^2) [4], which a plasma to form at the focus of the beam. This prevented the spatial filter from being used effectively. In the future a vacuum spatial filter could be used to improve the beam quality.

3.3. Open-Beam Experiments

Open-beam experiments were conducted to determine the laser intensity threshold to ablate a hole in the thin foil targets. The laser was focused to a 2 mm diameter spot on the foil. The laser was fired once and the target was removed and inspected. For laser energies below 19 mJ, no change to the foil was observed. At 19.3 +/- 0.5 mJ and 34 +/- 1 mJ the foil had an indentation at the location the laser hit. This likely indicates that the laser ablated some material from the surface of the foil, which applied a pressure to the rest of the foil. There was not enough laser energy to burn through the entire foil thickness though. At 42 +/- 1 mJ, a hole was observed in the foil.

Based on these results, the required laser energy density to burn through a 0.8 micron thick free-standing aluminum foil is between 11 and 13 mJ/mm^2. Based on this information, the required laser energy as a function of the spot size was calculated, and the results are plotted in figure 5. For a 600 µm diameter fiber, approximately 4 mJ must be coupled through the fiber. This is approximately 6 times the energy that was coupled through the fiber with a poor quality beam, but it is only a factor of 2 above the theoretical limit of 2.3 mJ.

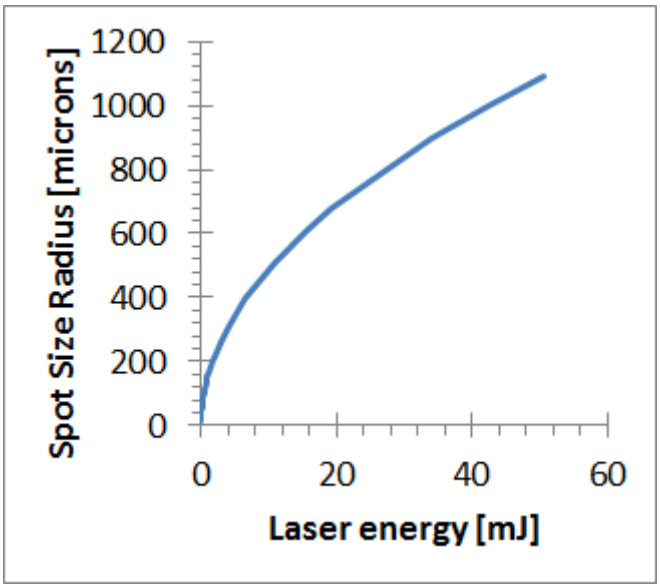

Figure 5. A plot of the maximum spot size as a function of laser energy that will punch a hole in a 0.8 µm thick aluminum foil.

The remaining experiments were conducted with solid targets to allow for many shots without changing targets. The laser spot size diameter was 2 mm, and the laser intensity was varied between 30 mJ and 100 mJ. The targets included a block of aluminum 5056 (5% magnesium), a thick copper foil (~100s of microns), and a sodium chloride/glue compound.

Open pinhole images of the experiment show a plasma plume expanding from the surface. Images that included the surface were saturated by scattered laser light as shown in figure 6, but a small modification to the setup shielded the camera from the scattered laser light. Images were collected for the copper and aluminum targets as shown in figure 7. The color of the plume is target dependent, which is expected based on the fact that aluminum has strong emission lines around 400 nm (deep blue) and copper has strong emission lines around 500 nm (blue-green).

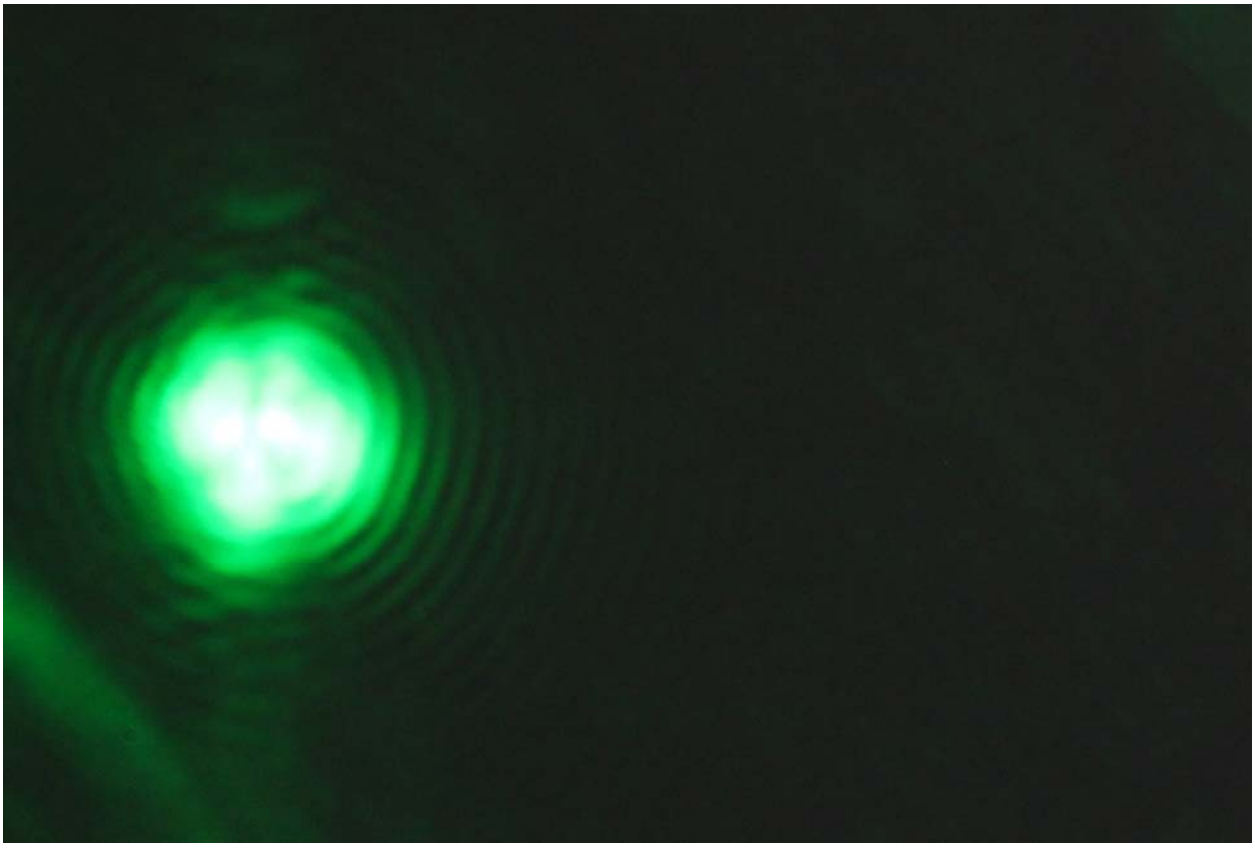

Figure 6. An open pinhole image of the laser striking the aluminum target and the resultant plasma plume. The scattered laser light is much brighter than the plasma plume so the plume is not observed.

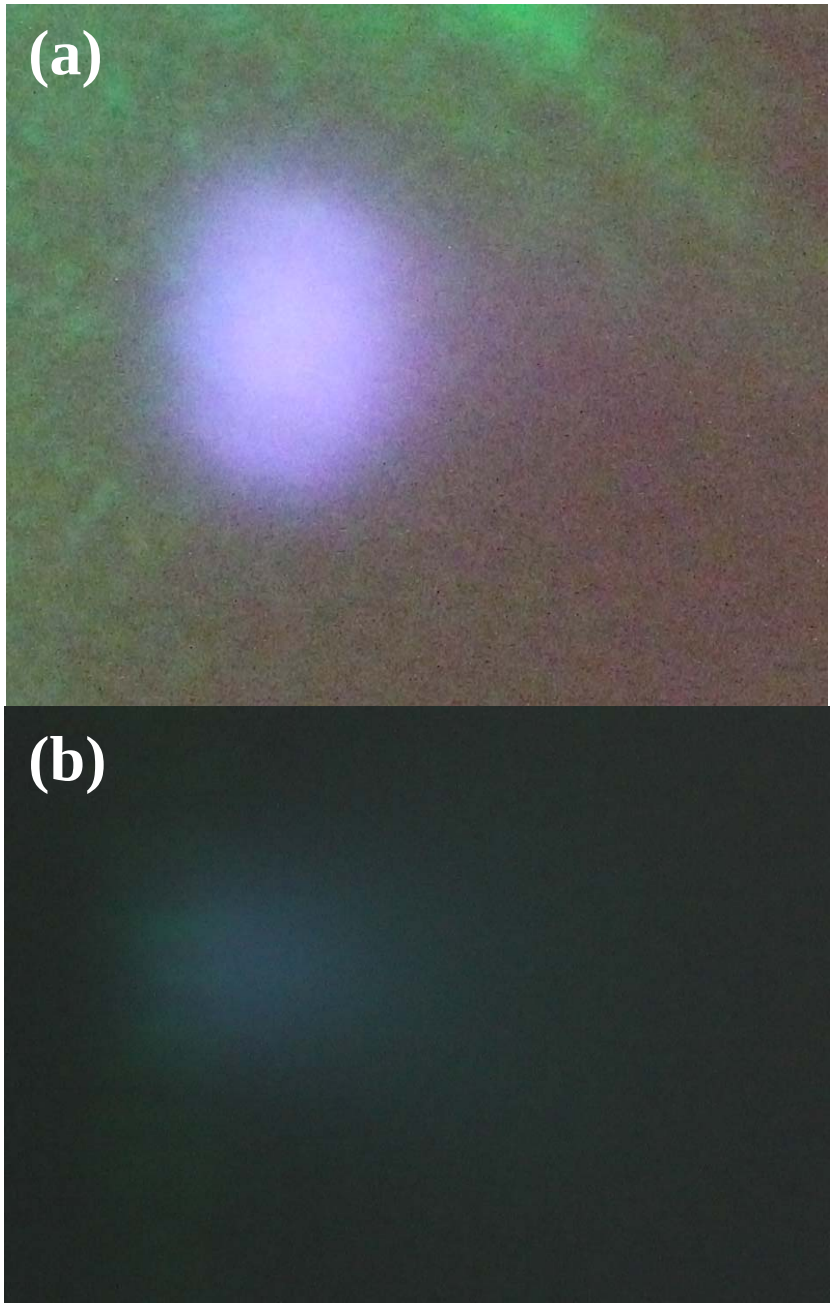

Figure 7. (a) An open pinhole image of the plasma plume from the aluminum target. The target has been modified to block out the scattered laser light and the camera sensitivity has been increased. (b) An open pinhole image of the copper target with the same modifications to the target and camera. Note that the aluminum plume is blue-violet and the copper plume is blue-green.

Time-resolved imaging of the plasma plume was attempted using laser shadowgraphy. A 150 mW diode laser with ~ 488 nm wavelength and a programmable pulse width was used as the source. Based on camera sensitivity and expected plume velocity, a 300 ns pulse was chosen. This gave a strong laser signal at the camera, and the expected motional blur of the plasma was expected to be less than 0.5 mm. Shadowgraphs were recorded at 1 μs intervals over a span of

20 µs. No evidence of plasma was observed in any of the images (see figure 8 for an example image). This is likely due to the diagnostic not being sensitive enough to observe the low density of the plasma. This issue could be resolved in future measurements by using a schlieren or interferometry system, which are more complicated to set up, but more sensitive to low densities.

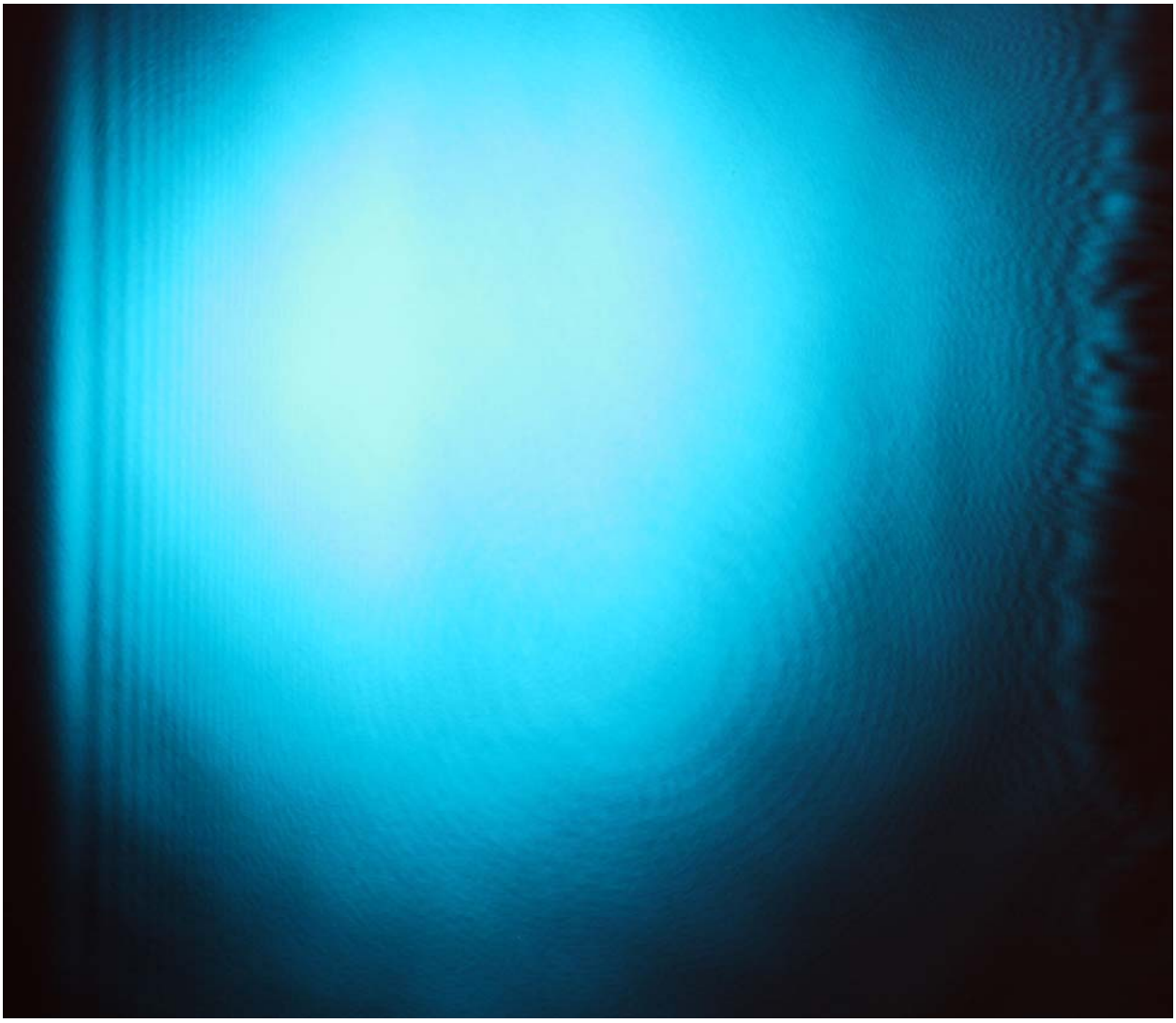

Figure 8. A shadowgraph of the aluminum target during a shot. The plume is not obvious in this image, which is likely due to the diagnostic not registering the low density plasma.

Time-integrated spectroscopic measurements of the three different targets were made. In each case emission lines were observed from the neutral state of the material. The aluminum spectrum had strong emission from the 394.4 nm and 396.2 nm lines, and emission was observed from the magnesium lines at 382.9 nm, 383.2 nm, and 383.8 nm. The magnesium emission was much weaker than the aluminum as expected since the concentration of aluminum in the target was nearly 20 times the magnesium concentration. A plot of the aluminum spectrum is shown in figure 9.

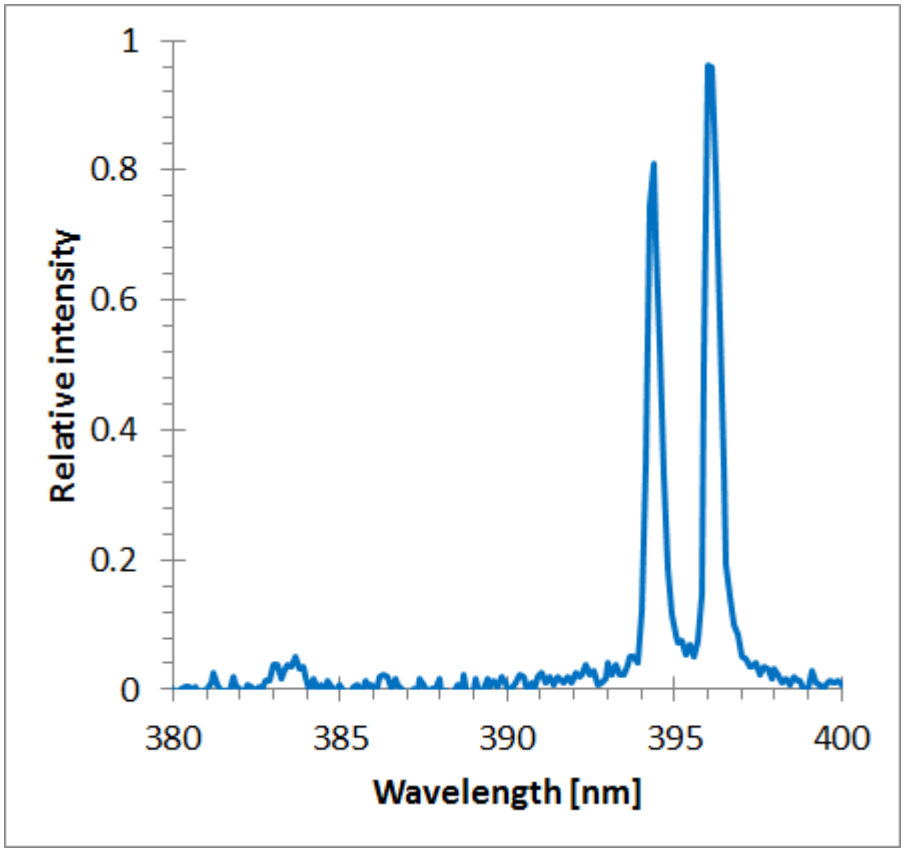

Figure 9. A plot of the spectrum from the aluminum 5056 target. Two strong aluminum neutral lines are observed around 394 nm and 396 nm, and 3 weak magnesium neutral lines are observed around 383 nm.

The copper target also showed strong emission from neutral lines. Neutral copper lines were observed at 510.6 nm, 515.3 nm, and 521.8 nm. The copper spectrum was slightly sloped upward at longer wavelengths as a result of the 532 nm laser line. This had a negligible effect on the spectrum. This spectrum is plotted in figure 10.

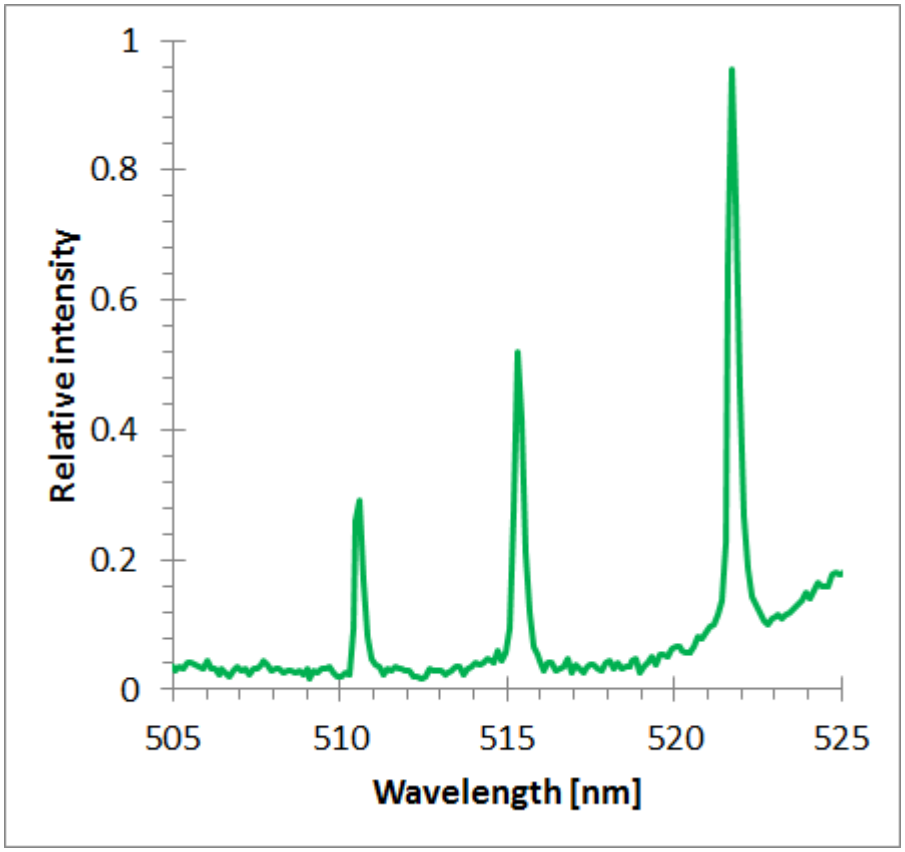

Figure 10. A plot of the spectrum from the copper target. Three strong copper neutral lines are observed around 510 nm, 515 nm, and 522 nm. The background slopes upward at the long wavelength end of the spectrum due to scattered laser light (532 nm).

The sodium target showed very weak emission from the neutral doublet at 589.0 nm and 589.6 nm. This could be due to a number of things. The sodium concentration is weaker than either of the other two materials because it is only 50% of the salt compound, and there is some packing factor of the salt and the glue in creating the target. This could negatively impact the target performance. The sodium could also be ionized in a greater fraction than the aluminum or the copper. A plot of the sodium spectrum is shown in figure 11. Note that the peaks in all of the plots have been normalized to unity, but the signal to noise gives an idea of the strength of the signals.

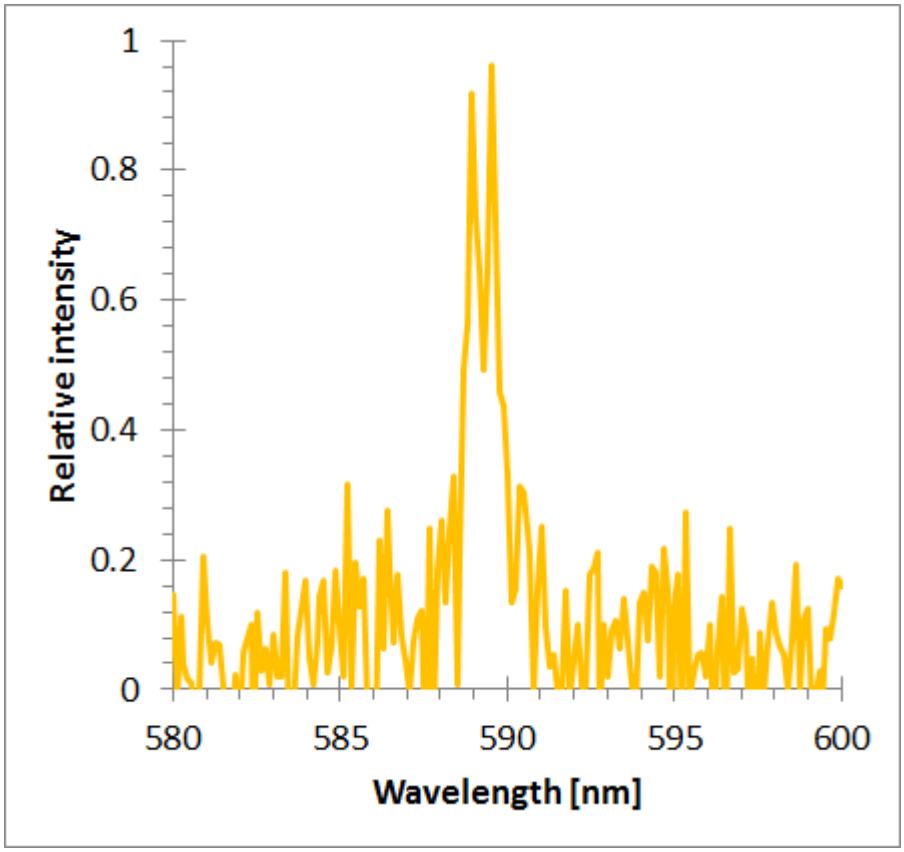

Figure 11. A plot of the spectrum from the sodium chloride and glue target. Two weak sodium neutral lines are observed around 589 nm. The signal to noise ratio for this target was only ~ 5.

4. CONCLUSIONS AND FUTURE WORK

Active doping through laser ablation appears promising. Open-beam experiments produced relevant plasma with solid targets, and an energy density threshold for foil ablation was determined as well. Fiber optic coupling of sufficient laser energy is not possible for the laser used in these experiments without modification. Vacuum spatial filtering may be the easiest path forward for fiber optic coupling. Additional work will be conducted to capture time-resolved images of the plasma plume. New targets will be tested, including new materials, a better solid sodium target, glass-backed foils, and dopants directly coated onto the end of fibers.

5. REFERENCES

1. S. Tessarin, D. Mikitchuk, R. Doron, E. Stambulchik, E. Kroupp, Y. Maron, D. A. Hammer, V. L. Jacobs, J. F. Seely, B. V. Oliver, A. Fisher, Phys. Plasmas **18**, 093301 (2011).
2. LEONI Fiber Optics, *Damage Resistance of FiberTech Fiber for High Power Laser Applications* (2011).
3. Arlee V. Smith, Binh T. Do, Applied Optics **47**, No. 26, pp. 4812-4832, (2008).
4. Magesh Thiyagarajan, Shane Thompson, J. Appl. Phys. **11**, 073302 (2012).

DISTRIBUTION

1	MS1189	Mark Herrmann	1680
1	MS1190	Greg Rochau	1675
1	MS1193	Mike Cuneo	1650
1	MS1193	Matt Gomez	1683
1	MS1193	Dan Sinars	1688
1	MS0359	D. Chavez, LDRD Office	1911
1	MS0899	Technical Library	9536 (electronic copy)

Sandia National Laboratories